Journal of Physical Science, Vol. 32(2), 27–39, 2021

Co-precipitation Synthesis with a Variation of the Sulphur Composition of Kesterite Phase Cu_2ZnSnS_4 (CZSS) without Annealing Process

Krishan Pal,[1] Dheeraj Kumar Maurya,[2] Priyanka Chaudhary,[1] Khem Bahadur Thapa,[1*] and Bal Chandra Yadav[1]

[1]Department of Physics, School of Physical and Decision Sciences, Babasaheb Bhimrao Ambedkar University (A Central University), Lucknow-226025 (UP), India
[2]Electro-materials Research Laboratory, Centre for Nanoscience and Technology, Pondicherry University, Puducherry-605014, India

[*]Corresponding author: khem.bhu@gmail.com

Published online: 25 August 2021

To cite this article: Pal, K. et al. (2021). Co-precipitation synthesis with a variation of the sulphur composition of kesterite phase Cu_2ZnSnS_4 (CZSS) without annealing process. *J. Phys. Sci*., 32(2), 27–39. https://doi.org/10.21315/jps2021.32.2.3

To link to this article: https://doi.org/10.21315/jps2021.32.2.3

ABSTRACT: *Commercially available compound CuInGa (S, Se) can be replaced with emerging quaternary compound Cu_2ZnSnS_4 (Copper Zinc Tin Sulphur or CZSS) for photovoltaic applications due to the high absorption coefficient and optimum bandgap. Unstable sulphur and the co-existence of binary and ternary phases in CZSS are the main obstacles for a single-phase kesterite quaternary compound. To overcome these issues, the researchers are synthesising the CZSS in presence of sulphur and selenium environment. The sulphurization and selenization are the constraints for the synthesis of CZSS and these processes make it costlier. In the present work, the wet-chemical method (i.e., co-precipitation method) was used to synthesise CZSS without vacuum annealing where the sulphur constituent was controlled by changing the stoichiometric ratio. X-ray diffraction (XRD) and Raman analysis confirm that the synthesised CZSS was in polycrystalline and single-phase kesterite nature. The average crystallite sizes for thiourea 16, 18, 20 mmol were found 15 nm, 17 nm and 17 nm, respectively. Surface morphology of the as-prepared film was identified by scanning electron microscope (SEM) and optical bandgap of the film was obtained ~1.33 eV by UV-visible (UV-vis) analysis. The 18 mmol of thiourea with stoichiometric ratio 4:2:2:9 is found the best optimisation for synthesising the CZSS without vacuum annealing by the co-precipitation method. Thus, the thin film of such synthesised CZSS may be employed for the low-cost photovoltaic application.*

Keywords: Cu_2ZnSnS_4, co-precipitation, without annealing, kesterite, photovoltaic

1. INTRODUCTION

In the last three decades, Cu_2ZnSnS_4 (CZSS) nanomaterials have attracted enormous attention by promising development for solar energy conversion due to high absorbent ($>10^4 cm^{-1}$), low cost, environment-friendly, non-toxic and sustainable earth-abundant elements. CZSS has a tunable bandgap of about 1.4 eV to 1.6 eV, which is very close to the optimum value as an absorber layer in solar cells.[1–3] According to the Shockley and Queisser limit, the bandgap range, 1.4 eV to 1.6 eV, is suitable for thin-film photovoltaic cells. On the other hand, CZSS is the counterpart of CuInGa (S, Se) (CIGS) because both Zn (+2) and Sn (+4) have similar properties to In (+6). But the co-existence of binary and ternary phases, the synthesis of CZSS puts a lot of hurdles in its development.[4] An effort has been laid by researchers to overcome the phase problem by sulphurization process in inert or vacuum atmosphere.[5,6] Such process also has a constraint of cost and time consumption. So, the exploration of novel methods for the CZSS synthesis has gained much attention across the globe.

To overcome the problems of the sulphurization process in an inert or vacuum atmosphere, many researchers have been used other methods for synthesising CZSS nanomaterial for wide applications such as photovoltaic, hydrogen generation and light emitting diode (LED), etc.[7] Co-precipitations, sol-gel, solvothermal, hot-injection, one-pot syntheses and microwave-assisted methods are widely adopted for purpose of the photovoltaic application.[5,6,8–11] In a design of a photovoltaic device, the CZSS material is used as an absorber layer.

According to previously reported results, the disadvantage of the device structure, Mo/Absorber layer/buffer layer/nanostructured metal oxide/metal grids, is highlighted with regard to the thermal instability in the absorber layer, which can be only controlled by buffer interface.[12] In addition to this limitation, photovoltaic cells in this configuration have erosion reaction between CZSS and Mo at back contact, and the surface instability of CZSS has increased during the heat treatment.[13] This drawback can be overcome by the deposition of metal oxide on a smooth surface of a substrate with subsequent annealing at high temperatures to prevent the direct contact of CZSS and the conducting substrate. It is evident from previous studies that, nanorods are the best substitute for metal grids.[14,15] Hence, the TiO_2 thin layer was offered the highest conversion efficiency of 0.25%.[16] Hamady et al. trying to develop a novel approach of InGaN Schottky based solar cell device to make the efficiency 22%, theoretically.[17] The CZSS may be a better option in place of GaN in this device.

In the present work, we have described a facile and low-cost synthesis of wurtzite CZSS Nanocrystals (NCs) without vacuum annealing or sulphurization by the

co-precipitation method where ethanol and water were used as a solvent. The co-precipitation method is done at room temperature without any surfactants and noble gases as well as vacuum process. Besides, this method does not require annealing the synthesised samples. As compared to other methods, this method is simple and economical. The formation of kesterite CZSS NCs, ethanol solvent plays an important role in the CZSS phase transition from a tetragonal structure and the balanced stoichiometry ratio of the compound optimizes sulphur content. The novelty in this work lies in the synthesis of NCs CZSS material by an economically cheaper co-precipitation method without any sulphurization and selenization because the sulphurization and the selenization processes in the NCs CZSS synthesis are imparted huge toxicity to the environment. Hence, the NCs are evident that the surface-to-volume ratio enhances the properties of the material. The high absorption coefficient and optimum bandgap of NCs CZSS can be synthesised by the co-precipitation method without sulphurization or vacuum annealing. The cost-effective thin film of CZSS NCs can be very useful to enhance the efficiency of the photovoltaic cells.

2. EXPERIMENTAL METHODS

2.1 CZSS NCs Powder Synthesis

The metallic Cu, Zn, and Sn cations were taken as the cupric (II) chloride ($CuCl_2.2H_2O$, Thermo Fisher Scientific India Pvt. Ltd., Maharashtra, India, 98.5%), zinc (II) acetate ($Zn[CH_3COOH]_2.2H_2O$, Thermo Fisher Scientific India Pvt. Ltd., Maharashtra, India, 98.5%), Stannous or tin (II) chloride ($SnCl_2$, Thermo Fisher Scientific India Pvt. Ltd., Maharashtra, India, 97%) and the sulphur anion was taken as thiourea (NH_2CSNH_2, Sarabhai Chemicals [India] Pvt. Ltd., Ahmedabad, India [reagent grade], 98%). In a typical experimental procedure, the preparation of metal precursor cupric (II) chloride (8 mmol, 0.5455 gram [gm.]), zinc (II) acetate (4 mmol, 0.3512 gm.), tin (II) chloride (4 mmol, 0.3034 gm.) were dissolved in 200 ml ethanol in a beaker. The reaction mixture was stirred continuously for 10 min at 400 round per minute (rpm). After that, thiourea (20 mmol, 0.6090 gm.) was added in 200 ml ethanol as a sulphur precursor and stirred well for 5 min, and mixed within the first beaker quickly. The reaction mixture was stirred continuously for 3.5 h and found a transparent homogeneous solution. Then, the mixture was transferred into an oven for 3 h at 210°C temperature and subsequently, it was cooled down to room temperature to obtain black colour precipitation. This precipitation was further centrifuged at 7,000 rpm for 15 min and washed several times by distilled water and ethanol, respectively. The schematic diagram is shown in Figure 1. Finally, it was dried at 80°C in the

oven and it was crushed into a fine powder using a mortar pestle, named sample A. Similar process was taken for 18 mmol (0.5480 gm.) and 16 mmol (0.4871 gm.) of sulphur in the salt thiourea and prepared the fine powder, named as samples B and C, respectively.

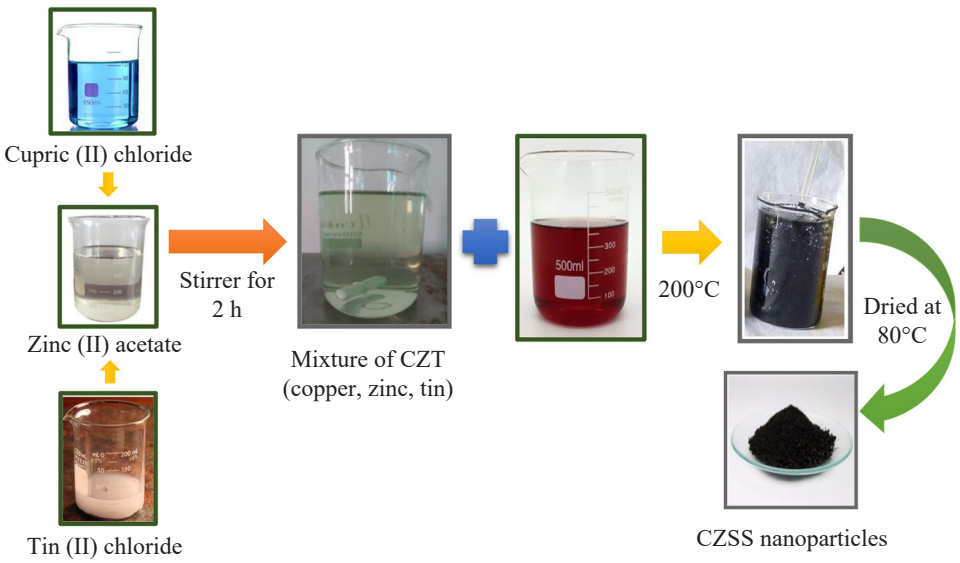

Figure 1: Schematic diagram for synthesis process of CZSS NCs.

2.2 Growth and Formation Mechanism

Generally, in this synthesis process, metal salts react with ethanol and form the metal alkoxide [M(Tu)m]-OR. Then, the nanocrystals are generated during the polycondensation reactions. In this process, thiourea reacts with metal ions and forms the metal thiourea complexes. The metal thiourea complexes are subsequently subjected to alcoholysis and condensation reactions with ethanol at 210°C and formed the CZSS nanocrystals. The probable reaction mechanisms are followed as:

$$M - X + \mathrm{Tu} \rightarrow [M(\mathrm{Tu})m] - X \tag{1}$$

$$[M(\mathrm{Tu})m] - X + ROH \rightarrow [M(\mathrm{Tu})m] - OR + H - X \tag{2}$$

$$M - X + \mathrm{Tu} \rightarrow [M(\mathrm{Tu})m] - X \tag{3}$$

$$[M(\mathrm{Tu})m] - X + ROH \rightarrow [M(\mathrm{Tu})m] - OR + H - X \tag{4}$$

$$[M(\mathrm{Tu})m] - X + [M(\mathrm{Tu})m] - OR \rightarrow [M(\mathrm{Tu})m] - O - [M(\mathrm{Tu})m] + R - X \tag{5}$$

$$[M(\mathrm{Tu})m] - O - [M(\mathrm{Tu})m] + R - X \rightarrow Cu_xS + ZnS + Sn_xS + SnO_2 + Volatile(matter) \quad (6)$$

$$Cu_xS + ZnS + Sn_xS \rightarrow Cu_2ZnSnS_4 \quad (7)$$

$$Cu_xS + ZnS + SnO_2 \rightarrow Cu_2ZnSnS_4 \quad (8)$$

The representation of the symbols (M, X, Tu, and R, x) in these equations are represented as M = metal ions (Cu^{2+}, Zn^{2+}, Sn^{2+}), X = anions (CH_3COO^- or Cl^-), Tu = thiourea and R = organic molecular chains of ethanol, x = quantity of elements. The gases CS_2, CO_2, NO_2, SO_2, H_2O, and NH_4Cl are volatile materials and generated during the synthesis process at 210°C. In organic solvents, thiourea–metal complexes [M(Tu)m]–X is easily generated from thiourea and metal ions (Cu^{2+}, Zn^{2+}, Sn^{2+}), and several complexes are reported with different stoichiometry.[18–19] In traditional non-aqueous nanoparticle synthesis routes, the oxygen in the formation of a metal–oxygen–metal bond is provided by the solvent or by the organic constituent of the precursor.[20] Generally, M–O bonds, M–S bonds, and O–M–S bonds of the thiourea–metal complex [M(Tu)m]–O–[M(Tu)m] system (as shown in Equations from 1–8) have coexisted in the precursor Sol-Gel method.[18]

2.3 Thin Film Preparation

The soda-lime glass (SLG) substrate was used to deposit the CZSS thin film by spin coater (HSC-8000) and this was used to analyse the scanning electron microscope (SEM). Before the deposition of the CZSS solution, the SLG substrate was cleaned by an ultrasonic bath in distilled water and ethanol and was dried at 80°C in an oven. The CZSS solution was prepared in ethylene glycol (EG) and found a homogeneous solution after ultra-sonication. The CZSS solution was deposited by spin coater at 1,000 rpm for 30 sec and was repeated this process three to five times to get the best thickness of the film. The CZSS film was dried in the oven at every process of deposition.

3. CHARACTERISATION TECHNIQUES

The structural characterisation of the CZSS NCs was analysed by Bruker D8 Advance X-ray diffractometer with 0.154056 nm wavelength of X-ray (Cu K-α radiation) in the angle range 20° to 70°. For optical properties, the spectroscopic measurements have measured the spectra of UV-visible (UV-vis) absorption using a UV-vis spectrophotometer (ThermoFisher Scientific, Massachusetts, USA, Evolution 201). Raman scattering patterns were performed by the Raman

spectrometer model (HORIBA France SAS, Loos, France Jobin-Yvon Lab RAMHR 800UV) and the wavelength 514 nm of the Raman spectrometer was used. The surface morphology of CZSS NCs was performed by SEM-JEOL (JEOL Ltd., Tokyo, Japan, JSEM-6490LV).

4. RESULTS AND DISCUSSION

4.1 X-ray Diffraction (XRD) Analysis

Figure 2 shows the XRD pattern of CZSS NCs in the range of diffraction angle 20° to 70°. The XRD pattern exhibits the signature of prominent peaks at angles (2θ) in 28.5°, 47.3° and 56.2° corresponds to the planes (112), (200) and (312), respectively. The XRD pattern of CZSS confirms standard tetragonal kesterite Cu_2ZnSnS_4 crystal structure with JCPDS card no. 26-0575. The XRD pattern reveals a minor presence of impurities or deformations in sample C because the low peak intensity corresponds to the plane (312). It is cleared from the XRD patterns of samples A and B that these samples are having less impurity as compared to sample C. This result suggests that sample A and sample B are free from any such impurities witnessing the formation of a pure kesterite phase. There is either a loss in crystallinity or a decrease in crystallite size because intensity and peak positions are varied slightly from sample A to sample C. The average crystalline size was to be found 15 nm, 17 nm and 17 nm, respectively by Debye-Scherrer's formula.

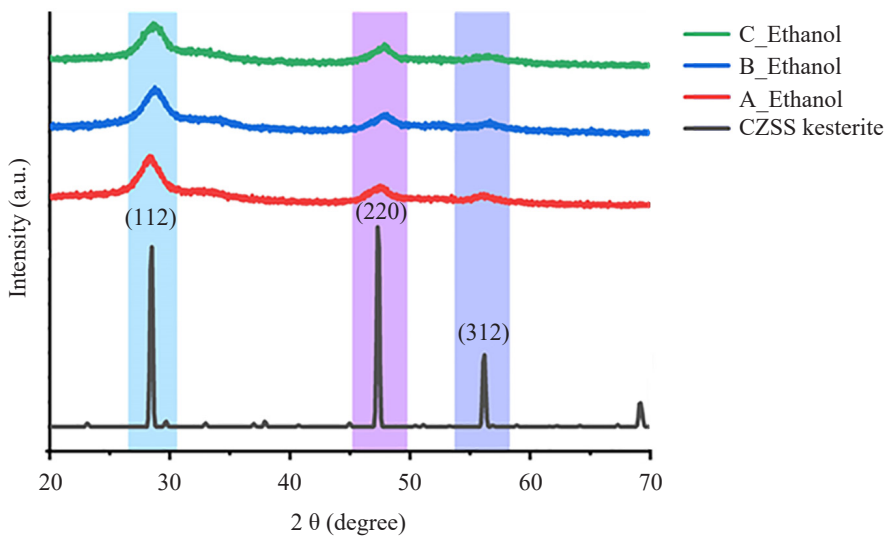

Figure 2: XRD patterns of CZSS samples A, B and C with the variation of concentration of sulphur, comparative with standard CZSS kesterite.

According to Cheng et al., their study showed that strong peaks of Cu_3SnS_4, Cu_4SnS_4, CuS, Cu_2S, SnS, SnS_2 were not found in XRD patterns which is similar to our XRD results.[19] So, it confirms that the synthesised CZSS NCs are in the pure quaternary phase in nature. However, at a first glance, XRD patterns of CZSS, CSS and ZnS are indistinguishable because the peak (220) in the CSS and ZnS has the same as the peak (220) in the CZSS. For adequate phase formation identifications in CZSS samples, further analysis is required. Therefore, Raman spectroscopy of the samples A, B, and C has been done to differentiate the phases of CZSS, CSS, and ZnS materials.

4.2 Raman Spectroscopy

The presence of spatial distributions of various chalcogenide phases can be distinguished by Raman spectroscopy. Minute differences in the phonon densities of states between the different chalcogenide phases can be distinguished from the shifting peaks in the Raman scattering of the samples. According to Himmrich and Haeuseler, CZSS and its phases have distinguished by studying the Raman spectra and identified a strong peak at 336 cm^{-1} and two weak peaks at 285 cm^{-1} and 365 cm^{-1}.[21] Recently, lots of review literature reports on the Raman spectrum of CZSS have been published where the most intense peak position is found at 332–339 cm^{-1} and weak peak positions at 251–288 cm^{-1} and 368–374 cm^{-1}.[22–23] The strong Raman peak of the CZSS is associated with the strong Raman peak of the ternary chalcogenide compounds Cu_2SnS_3 and Cu_3SnS_4.[24]

Figure 3 shows the Raman spectrum of chalcogenide CZSS nanocrystals, which was synthesised through the homemade simple method without any surfactant. In this figure, Raman spectra are compatible with the XRD results because XRD data was confirmed that the prepared CZSS NCs are tetragonal kesterite structures. In the Raman spectrum, this confirmation is justified by high intensity (major) peaks at 328 cm^{-1}, 332 cm^{-1}, 333 cm^{-1} with two shoulder peaks at 288 cm^{-1} and 351 cm^{-1}, 352 cm^{-1}, 355 cm^{-1} for prepared samples A, B and C, respectively. Generally, quaternary compounds of the metal sulphides form unstable sulphur and co-existence of binary and ternary phases. From the Figure 3, it can be observed a good peak results for the case without annealing of the samples. The reason is that the access quantity of sulphur has been taken in optimisation conditions. In this process, the excess sulphur supply evaporates sulphur and maintains the stoichiometric ratio. Some minor peaks are identified with less intensity at 475 cm^{-1} and 575 cm^{-1}. These minor peaks confirm that there may be the phases of Cu_2SnS_3 and ZnO.[25] But XRD characteristics already verified that such compounds do not exist.

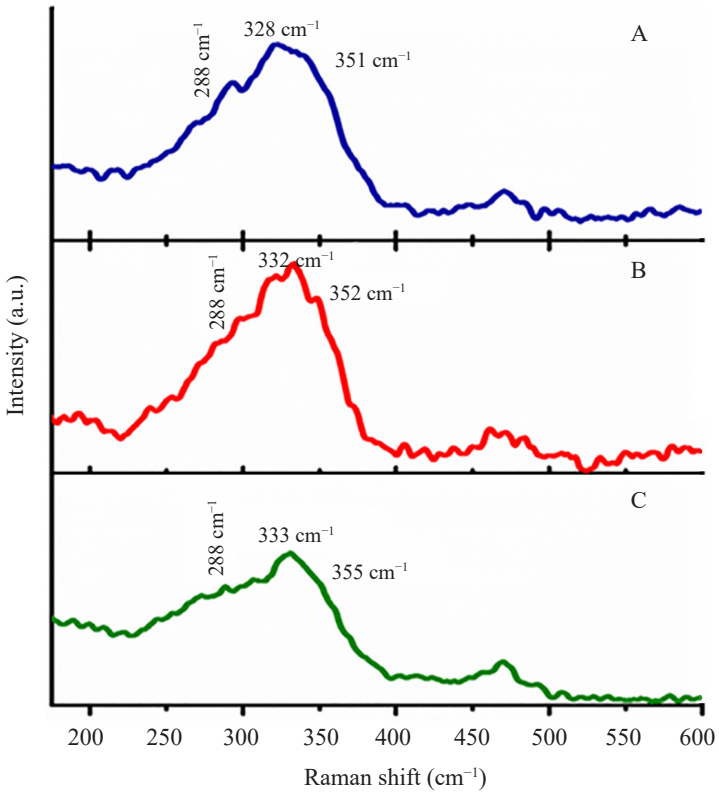

Figure 3: Raman spectra of CZSS kesterite (NCs) synthesised from Cu^{2+}, and Sn^{2+} at 210°C while varying the S:M ratio. The sulfur source thiourea was varied from 16 mmol, 18 mmol, 20 mmol, i.e., samples A, B and C, respectively.

From Figure 3, we confirm that the peak intensities of Raman spectroscopy are shown lower and broader. The broadening of peaks in nanocrystalline materials is usually described by the phonon confinement model as explained by XRD results due to crystalline size (15 nm to 17 nm). The phonon confinement leads to a break-up of selection rules; it also means that the non-zone-centre phonons will participate in scattering.[21] This usually can be seen in an asymmetric broadening of peaks. However, it is common to observe that the peaks are shifted towards the higher wavenumbers (e.g., 332 cm^{-1} to 333 cm^{-1}). According to the review literature, the peak of sample A has the wave number 328 cm^{-1}, which is out of the wavenumber range 331 cm^{-1} to 339 cm^{-1}.[22–23] So, we can say that this sample A is not in a pure form of stoichiometric range. So, it may not be useful for photovoltaic applications. The inhomogeneity in the structure is due to the disordered cation within the sublattice that is detected by peak shifting towards the higher angle side. Peaks related to secondary phases such as Cu_2S, SnS, SnS_2, ZnS, Cu_2SnS_3;

and Cu_3SnS_4 were not detected. Some of these compounds (ZnS, Cu_2SnS_3 and Cu_3SnS_4) have found partially overlapping peaks with CZSS. After analysing the XRD and Raman characterisations, we conclude that sample B has given the best results due to the proper stoichiometric ratio for a stable CZSS compound. The morphology of the samples is studied by SEM.

4.3 SEM Analysis

For the SEM analysis, we have mounted the sample on a mounting stand with the help of carbon tape. After mounted the sample, the platinum (Pt) was coated. Figure 4(a), 4(b) and 4(c) show the surface morphology of CZSS NCs thin film with the variation of sulphur quantity. The morphology of sample A shows spherical type nanoparticles that are distributed roughly on the SLG substrate and identified the more cracks in the film. There are more agglomerated crystals and it is identified agglomeration. In samples B and C, it has been observed that the size and shape NCs are changed. In these samples, the agglomerations are less and the films are less cracked compared to sample A.

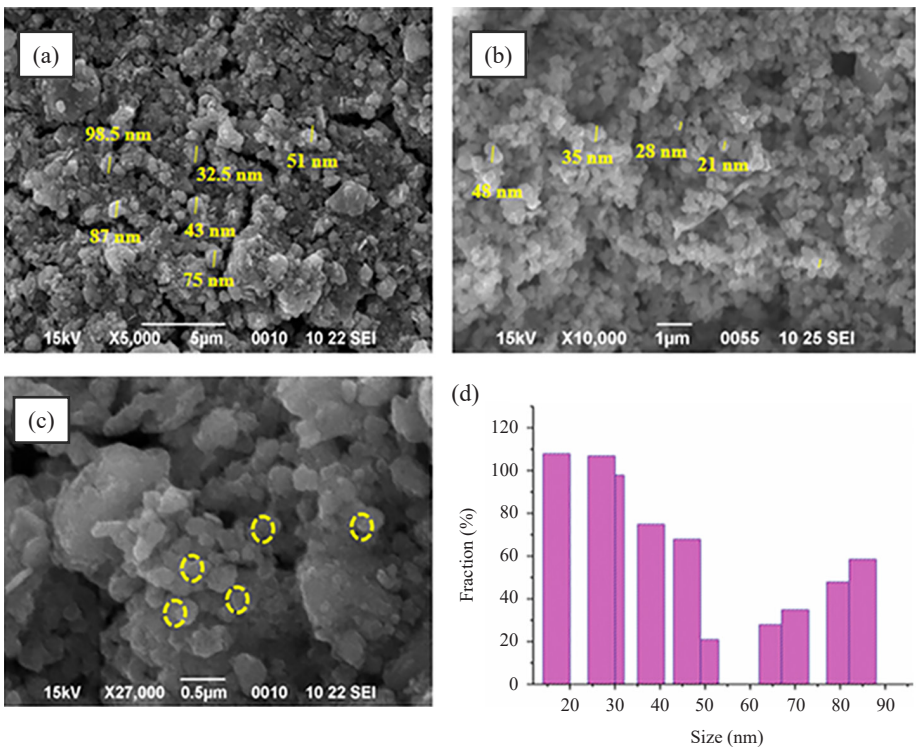

Figure 4: (a), (b), (c) SEM images of CZSS powder thin film with samples A, B and C, respectively, and (d) size distribution with fraction percentage.

The problem of cracking in the film is due to the solvent evaporation rate, which may be removed by changing the evaporation rate. Here, agglomeration is generated due to the anisotropic growth of materials during film fabrication. During the synthesis process, anisotropic growth is being found due to the selective binding nature of ligands. The obtained result confirms that the crystal growth has improved from sample A to sample C as the variation of sulphur is increased. Here, we have analysed the surface morphology at different resolutions because the surface is not showing the clean surface at the same resolution. Figure 4(d) explains the size distribution of the CZSS nanocrystals of sample B with the fraction percentage. This figure confirms that how the size of the NCs distributed in the film. Due to having a good phase and morphology in sample B, the optical bandgap was analysed only to see the suitability for the application of the photovoltaic cells.

4.4 Optical Analysis

The good phase and morphology in the sample B were analysed by the XRD and Raman analysis. So, we have decided to characterise the optical analysis of sample B only by UV-vis spectrometer. The optical bandgap of sample B is shown in Figure 5. The energy of the optical bandgap was analysed by using the formula $\alpha = A(h\nu - E_g)^{1/2}/h\nu$.

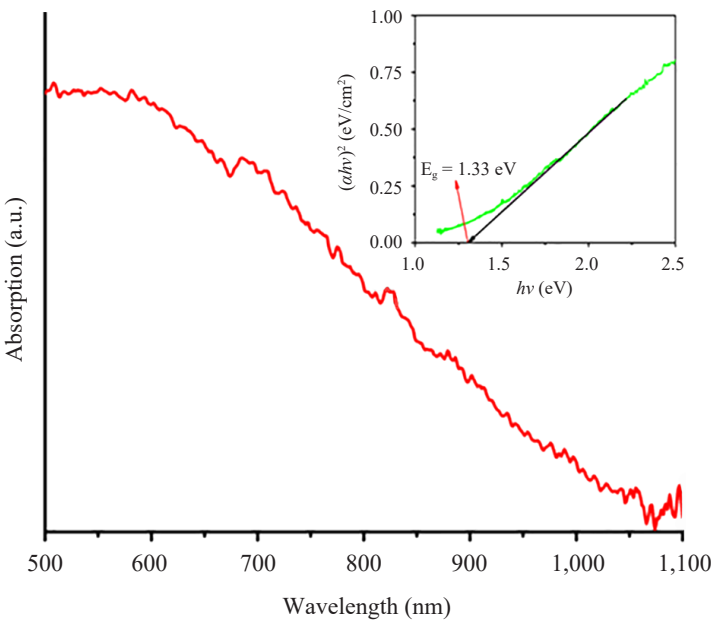

Figure 5: UV-vis absorption spectrum of the CZSS NCs. Inset shows the plot of $(\alpha h\nu)^2$ vs. $h\nu$.

After analysing, the bandgap is to be found 1.33 eV, which is suitable for photovoltaic cell application. Shockley and Queisser theoretically announced that such bandgap limit should be ≈1.5 eV for the highly efficient photovoltaic cell. So, the calculated bandgap of sample B is covered in this range and sample B is highly suitable for a photovoltaic cell. Besides this, the XRD analysis has been shown that the Cu_2SnS_3 and ZnO phases do not exist which is confirmed by the optical spectroscopy characteristics. The novelty in this work lies in the synthesis of CZSS NCs by an economically cheaper co-precipitation method without any sulphurization and salinization processes. In the absence of sulphurization and salinization processes, it imparts less toxicity to the material as well as the environment. The nanocrystals of CZSS have enhanced the surface to volume ratio properties of the synthesised material. The single quaternary phase, good surface morphology, suitable optical bandgap in the sample B having CZSS nanocrystals may be a very useful material for photovoltaic cell application.

5. CONCLUSION

In this article, we synthesised the CZSS nanocrystals with sulphur variation of the 16 mmol, 18 mmol and 20 mmol thiourea by the co-precipitation method. The spin coater was used to fabricate the thin-films as samples A, B, C and such thin films have been used to analyse the surface morphology of all samples. After the XRD, Raman, and SEM characterisations of the samples A, B and C, it was confirmed that the sample B with 18 mmol thiourea concentration was found the best optimisation with the polycrystalline kesterite phase having the better morphology than the samples A and C. The average crystalline size of sample B was found at 17 nm. The calculated optical band gap of the sample B by UV-vis characterisation was showed the suitable for electron-hole generations. These exciting results demonstrate that the synthesised CZSS NCs by co-precipitation method without sulphurization may be fulfilled the promise of a low-cost thin film for photovoltaic cell application. The novelty of this work lies in the synthesis of CZSS nanocrystals by co-precipitation method without any sulphurization and selenization processes, which is less toxic to the material as well as the environment. By the characterisations analysis of the CZSS NCs of sample B, it has been revealed that the thin film of the CZSS NCs is the economically cheapest and the best material for photovoltaic cell applications.

6. ACKNOWLEDGEMENTS

Mr. Krishan Pal would like to thank University Grant Commission (UGC), New Delhi, India for the financial support through the Rajiv Gandhi National fellowship (F1-17.1/2015-16/RGNF-2015-17-SC-UTT-25302).

7. REFERENCES

1. Katagiri, H. (2005). Cu_2ZnSnS_4 thin film solar cells. *Thin Solid Films*, 480−481, 426−432. https://doi.org/10.1016/j.tsf.2004.11.024
2. Katagiri, H. et al. (2008). Enhanced conversion efficiencies of Cu_2ZnSnS_4-based thin film solar cells by using preferential etching technique. *Appl. Phys. Express*, 1, 041201. https://doi.org/10.1143/APEX.1.041201
3. Zhou, Y. L. et al. (2011). Hierarchical Cu_2ZnSnS_4 particles for a low-cost solar cell: Morphology control and growth mechanism. *J. Phys. Chem. C.*, 115, 19632−19639. https://doi.org/10.1021/jp206728b
4. Collord, A. D. & Hillhouse, H. W. (2015). Composition control and formation pathway of CZTS and CZTGS nanocrystal inks for kesterite solar cells. *Chem. Mater.*, 27, 5, 1855–1862. https://doi.org/10.1021/acs.chemmater.5b00104
5. Sun, Y. et al. (2013). Reaction routes for the formation of a Cu_2ZnSnS_4 absorber material from homogenous ethanol-based solution. *RSC Adv.*, 44, 22095–22101. https://doi.org/10.1039/C3RA42746C
6. Diamond, A. M. et al. (2012). Copperalloyed ZnS as a p-type transparent conducting material. *Phys. Status Solidi A.*, 209(11), 2186–2194. https://doi.org/10.1002/pssa.201228181
7. Bai, X., Milton, F. P. & Gun'ko, Y. K. (2019). Optical properties, synthesis, and potential applications of Cu-based ternary or quaternary anisotropic quantum dots, polytypic nanocrystals, and core/shell heterostructures. *Nanomaterials*, 9, 85–121. https://doi.org/10.3390/nano9010085
8. Su, Z. et al. (2014). Fabrication of Cu_2ZnSnS_4 solar cells with 5.1% efficiency via thermal decomposition and reaction using a non-toxic sol-gel route. *J. Mater. Chem. A*, 2, 500–509. https://doi.org/10.1039/C3TA13533K
9. Liu, W. C. et al. (2013). Facile hydrothermal synthesis of hydrotropic Cu_2ZnSnS_4 nanocrystal quantum dots: Band-gap engineering and phonon confinement effect. *J. Mater. Chem.*, 1, 3182–3186. https://doi.org/10.1039/C3TA00357D
10. Guo, Q., Hillhouse, H. W. & Agrawal, R. (2009). Synthesis of Cu_2ZnSnS_4 nanocrystal ink and its use for solar cells. *J. Am. Chem. Soc.*, 131, 11672–11673. https://doi.org/10.1021/ja904981r
11. Li, M. et al. (2012). Synthesis of pure metastable wurtzite CZTS nanocrystals by facile one-pot method. *J. Phys. Chem. C.*, 116, 26507−26516. https://doi.org/10.1021/jp307346k
12. Pal, K. et al. (2019). Current challenges and future prospects for a highly efficient (> 20%) kesterite CZTS solar cell: A review. *Sol. Energy Mat. Sol. Cells*, 196, 138–156. https://doi.org/10.1016/j.solmat.2019.03.001

13. Scragg, J. J. et al. (2013). Effects of back contact instability on Cu_2ZnSnS_4 devices and processes. *Chem. Mater.*, 25, 3162–3171. https://doi.org/10.1021/cm4015223
14. Pandey, G. & Srivastava, S. K. (2006). A novel synthetic method for the preparation of CuS, and CdS nanochains. *Synthesis and Reactivity in Inorganic, Metal-Organic and Nano-Metal Chemistry*, 36, 663–666. https://doi.org/10.1080/15533170600962455
15. Shrivastava, S. et al. (2010). Study of structural and electronic properties of metallic nanowires: Bi, Na, Cu, Pb. *Journal of Physics: Conference Series*, 245, 012089–012093. https://doi.org/10.1088/1742-6596/245/1/012089
16. Yan, R. et al. (2018). Solution-processed Cu_2ZnSnS_4 thin film with mixed solvent and its application in superstrate structure solar cells. *RSC Adv.*, 8, 11469–11477. https://doi.org/10.1039/C8RA01095A
17. Hamady, S. O. S. et al. (2019). Development of novel thin film solar cells: Design and numerical optimisation. *J. Phys. Sci.*, 30(2), 199–205. https://doi.org/10.21315/jps2019.30.s2.17
18. Smolander, K. et al. (1994). Monomeric (dipropionato-*O*)(dithiourea-*S*) zinc(II). *Acta Crystallogr. Sect. C*, 50, 1900–1902. https://doi.org/10.1107/S0108270194004397
19. Cheng, A. J. et al. (2011). Imaging and phase identification of Cu_2ZnSnS_4 thin films using confocal Raman spectroscopy. *J. Vac. Sci. Technol. A*, 29(5), 051203–051214. https://doi.org/10.1116/1.3625249.
20. Niederberger M. (2007). Nonaqueous sol-gel routes to metal oxide nanoparticles, *Acc. Chem. Res.*, 40(9), 793–800. https://doi.org/10.1021/ar600035e.
21. Himmrich, M. & Haeuseler, H. (1991). Far infrared studies on stannite and wurtzstannite type compounds. *Spect. Chim. Acta Part A: Mol. Spect.*, 47(7), 933–942. https://doi.org/10.1016/0584-8539(91)80283-O
22. Wang, K. et al. (2010). Thermally evaporated Cu_2ZnSnS_4 solar cells. *Appl. Phys. Lett.*, 97, 143508–143511. https://doi.org/10.1063/1.3499284
23. Woo, K., Kim, Y., & Moon, J. (2012). A non-toxic, solution-processed, earth-abundant absorbing layer for thin-film solar cells. *Energy Environ. Sci.*, 5, 5340–5345. https://doi.org/10.1039/C1EE02314D
24. Fernandes, P. A., Salomeand, P. M. P., & da Cunha, A. F. (2010). A study of ternary Cu_2SnS_3 and Cu_3SnS_4 thin films prepared by sulfurizing stacked metal precursors. *J. Phys. D: Appl. Phys*., 43(21), 215403–215411.
25. Rakhshani, A. E. (2020). Sn-rich CZTS films spin-coated from methanol-based sol-gel solution: Annealing effect on microstructure and optoelectronic properties. *J Solgel Sci Technol.*, 94, 270–278. https://doi.org/10.1007/s10971-020-05262-7.